# Boundary Element Method Analysis of 3D Effects and Free-Surface Proximity on Hydrofoil Forces in Varied Operating Conditions

**Conference Paper** · May 2023

CITATIONS
0

READS
86

**4 authors:**

Hugo Nicolas
University of Michigan
**1** PUBLICATION **0** CITATIONS
SEE PROFILE

Paolo Perali
ENSTA Bretagne
**7** PUBLICATIONS **22** CITATIONS
SEE PROFILE

Matthieu Sacher
ENSTA Bretagne
**33** PUBLICATIONS **181** CITATIONS
SEE PROFILE

Patrick Bot
Ecole Navale de Lanvéoc-Poulmic
**60** PUBLICATIONS **570** CITATIONS
SEE PROFILE

# Boundary Element Method Analysis of 3D Effects and Free-Surface Proximity on Hydrofoil Forces in Varied Operating Conditions

**Hugo Nicolas**
IRENav, École Navale, France.

**Paolo Perali**
ENSTA Bretagne, CNRS UMR 6027, IRDL, France.

**Matthieu Sacher**
ENSTA Bretagne, CNRS UMR 6027, IRDL, France.

**Patrick Bot**
IRENav, École Navale, France, patrick.bot@ecole-navale.fr

**Abstract.** The use of hydrofoils as a means to improve ship performance raises the scientific issue of free-surface proximity, which must be considered in the design stage to feed velocity prediction programs, for instance. When predicting performance, it is convenient, for a selected accuracy level, to minimize the computational cost of models. Therefore, the present paper investigates the reliability of estimating the hydrodynamic characteristics of 3D wings using 2D simulations. In particular, the influence of aspect ratio on the hydrodynamic characteristics of shallowly-submerged hydrofoils under different operating conditions is addressed. For this purpose, rectangular wings (H105 profile at $2^\circ$ angle of attack) of an aspect ratio between $4$ and $20$ are systematically analyzed using a 3D boundary element method. The free surface is modeled using a linearized Neumann-Kelvin condition. For the three chord-based Froude numbers studied ($Fr_c = 0.5$, $Fr_c = 1.1$, and $Fr_c = 6.3$), the submergence depth is swept between $0.1$ and $30$ times the foil chord. The trend of the hydrodynamic forces with respect to foil immersion for each Froude number is discussed in detail. The convergence of lift and drag with an increase in aspect ratio is observed. It is identified that the latter is accelerated with free-surface proximity at $Fr_c = 6.3$, suggesting the existence of a relationship between the depth of immersion and the speed of convergence. All in all, this work validates the application of steady boundary element methods for simulating the flow around a hydrofoil wing in the vicinity of the free surface and lays the foundations for an extensive study of the influence of geometrical parameters on hydrofoil performance.

**Keywords:** hydrofoil; free surface; aspect ratio; potential flow; boundary element method (BEM).

## NOMENCLATURE

| | |
|---|---|
| $c$ | Hydrofoil root chord length [m] |
| $C_D$ | Drag coefficient [m] |
| $C_{D_0}$ | Reference drag coefficient [m] |
| $C_L$ | Lift coefficient [m] |
| $C_{L_0}$ | Reference lift coefficient [m] |
| $Fr_c$ | Chord-based Froude number [-] |
| $g$ | Gravitational acceleration [m $s^{-2}$] |
| $h$ | Submergence depth [m] |
| $\boldsymbol{n}$ | Vector normal to the domain boundary [m] |
| $r$ | Distance to velocity potential [m] |
| $S$ | Surface of the domain boundary [$m^2$] |
| $S_B$ | Body surface of the domain boundary [$m^2$] |
| $S_{FS}$ | Free surface of the domain boundary [$m^2$] |
| $S_W$ | Wave surface of the domain boundary [$m^2$] |
| $\boldsymbol{u}$ | Velocity field vector [m $s^{-1}$] |
| $U_0$ | Undisturbed flow velocity in the $x$-direction [m $s^{-1}$] |
| $\boldsymbol{U_0}$ | Undisturbed flow velocity vector [m $s^{-1}$] |
| $(x, y, z)$ | Cartesian coordinate system [m, m, m] |

| | |
|---|---|
| $\alpha$ | Hydrofoil angle of attack [°] |
| $\alpha_0$ | Zero-lift hydrofoil angle of attack [°] |
| $\eta$ | Free-surface elevation [m] |
| $\Lambda$ | Wing aspect ratio [-] |
| $\Lambda_c$ | Critical wing aspect ratio [-] |
| $\mu$ | Doublet [m $s^{-1}$] |
| $\phi$ | Perturbation velocity potential [$m^2$ $s^{-1}$] |
| $\sigma$ | Source [$m^2$ $s^{-1}$] |

| | |
|---|---|
| BEM | Boundary element method |
| LLT | Lifting line theory |
| RANS | Reynolds-average Navier-Stokes |
| VLM | Vortex lattice method |
| VPP | Velocity prediction program |

## 1 INTRODUCTION

Hydrofoils are used to either partially or fully lift yachts and crafts to mitigate hydrodynamic resistance and improve seakeeping by reducing waterplane area, improving ship performance while reducing energy consumption. Thus, they find applications in the maritime sector, from sailboat racing to commercial shipping. Whether surface-piercing or fully submerged, these appendages typically operate close to the free surface. The question of free-surface proximity is of high importance even so that the influence of the vicinity with the free surface on hydrofoil characteristics must be considered in the design stage (Bal et al., 2001). Recently, the importance of accounting for free-surface proximity in performance prediction has been demonstrated through the implementation of a velocity prediction program (VPP) for the America's Cup AC75 yachts (Patterson and Binns, 2022).

To understand the influence of free-surface proximity, the physics of the problem may be studied using simulations of different levels of fidelity (e.g., lifting-line theory (LLT), vortex lattice method (VLM), panel method, Reynolds-average Navier-Stokes (RANS) solver) and experiments.

In previous studies, it was observed that the proximity with the free surface alters the flow field compared to an unbounded flow, which may significantly alter hydrofoil performance (Zhu et al., 2006; Bal, 2007). That is, the low pressure on the suction side of a shallowly-submerged lifting surface deforms the free surface, generating a transverse wave (Parkin et al., 1955). As shown by Kwag and Mori (1991), the resulting flow field appears drastically dependent on the dominant problem parameters. Those parameters are the chord-based Froude number $Fr_c$ (see Section 2 for definition), the submergence depth-to-chord ratio $h/c$, and the foil angle of attack $\alpha$.

The characteristic change in the wave pattern from subcritical Froude numbers ($Fr_c < 1.0$, where the gravitational forces dominate) to supercritical Froude numbers ($Fr_c > 1.0$, where the inertial forces dominate) is well described in scientific literature, particularly on 2D profiles (Yasko, 1998; Chen, 2012; Carabineanu, 2014). For supercritical Froude numbers, the wave is generated above the foil, thus increasing the gap between the appendage and the free surface (Bai, 1978). Contrary to a Venturi channel, the flow is slowed down by the free surface (Jego, 2022). This induces a significant decrease in the lift as the body approaches the free surface (Daskovsky, 2000). For low and moderate chord-based Froude numbers, however, the behavior is dependent on the submergence depth-to-chord ratio. Karim et al. (2014) showed that wave amplitude is impacted by immersion depth. In addition, the position of the wave itself depends on $h/c$. Too close to the free surface, the transverse wave crest is located right above the foil while its first trough is positioned downstream, leading to a decrease in lift-to-drag ratio (Pernod et al., 2023). When moving away from the very vicinity of the free surface, close to a critical value of $h/c$, the wave crest may move upstream of the foil while the trough remains downstream (Uddin and Karim, 2017). At such Froude numbers, the free surface acts like a rigid wall (Faltinsen, 2005). As a result, the flow above the suction side is accelerated analogously to a ground effect (Kwag and Mori, 1991). The increase in wave steepness may lead to wave breaking (Duncan, 1983). In that case, breaking waves are unsteady and lead to fluctuations in both lift and drag (Prasad et al., 2015). At a high angle of attack, this phenomenon may even prevent flow separation and delay stall (Ni et al., 2021). Consequently, hydrofoil lift increases until a critical value of $h/c$, before plummeting when approaching too close to the free surface (Filippas and Belibassakis, 2014). Regarding drag, a sharp peak preceding drag reduction was identified with respect to $h/c$ (Bal et al., 2001). The occurrence of the latter is independent of the flow regime, and its amplitude decreases with flow velocity (Xie and Vassalos, 2007). Such drag mitigation is significant, as Plotkin (1975) observed that the drag coefficient is highly damped at low Froude numbers. Above all, the effects of free-surface proximity vanish from a threshold value of submergence (Ali and Karim, 2010). Immersion depth can be thus considered infinite above the latter, thereby recreating deep water conditions (Hoque et al., 2017).

The evolution of the lift coefficient with respect to the Froude number is characteristic of the problem of free-surface proximity, up to the extent that it served as a reference for validating numerical models on a circular cylinder against the result of Havelock (1929) (Giesing and Smith, 1967). The consequences of the changes in wave pattern between $Fr_c < 1.0$ and $Fr_c > 1.0$ on the lift coefficient was illustrated by Yeung and Bouger (1979) based on a hybrid integral-equation method. Kennell and Plotkin (1984) further showed that the lift coefficient is maximum when operating at a subcritical Froude number close to the critical $h/c$. It was also observed that the lift coefficient remains practically unchanged above $Fr_c = 10$ (Hough and Moran, 1969). Subsequently, Hough and Moran (1969) selected $Fr_c \in [3, 10]$ as the range of interest for high-speed operating conditions.

Concerning the influence of the angle of attack on the hydrodynamic characteristics of a hydrofoil, Wadlin et al. (1952) showed that the lift evolves linearly with the angle of attack (until stall), with the slope of $C_L(\alpha)$ increasing with speed. Wadlin et al. (1952) also observed that the higher the speed, the higher the drag coefficient with respect to $\alpha$. In addition, the evolution of the drag coefficient is quadratic with respect to $C_L$, as discussed by Binns et al. (2008). Binns et al. (2008) also demonstrated no drawbacks of increasing heel angle on lift-to-drag ratio and unveiled the occurrence of

ventilation under extreme sailing conditions dependent on $\alpha$, $h/c$, and $Fr_c$.

While the general effects of free-surface proximity are still the subject of ongoing research, the question of how these effects are influenced by the foil geometry received less attention. In particular, limited knowledge is available on the influence of the wing aspect ratio on the performance alteration in the vicinity of the free surface. The first studies analyzed the effect of hydrofoil geometry on hydrodynamic characteristics using a lifting-line approach (Michel et al., 1954). A VLM solver allowed the investigation of the influence of the aspect ratio, taper ratio, sweep angle, and dihedral angle of a hydrofoil wing in close proximity to a free surface. Simulations on rectangular wings of aspect ratios up to $10$ under fixed operating conditions but $Fr_c \in [0 - 20]$ revealed that the lift and drag coefficients converge drastically faster with respect to the aspect ratio when speed is reduced up to $Fr_c = 1.0$ (Thiart, 2001). Yet, no submergence depths other than $h/c = 0.5$ was investigated. An iterative boundary element method validated against measurements on a spheroïd Farell (1973) revealed a significant decrease in drag induced by an increase in aspect ratio, at subcritical Froude numbers (Bal, 2007). A panel method was used to compute the lift coefficient on foils of aspect ratios $4$, $5$, and $6$ at a low Froude number (Xie and Vassalos, 2007). The same level of fidelity allowed to compute the wave field and hydrodynamic performance of closely-submerged hydrofoils with an aspect ratio between $4$ and $8$ operating at low and moderate Froude numbers at $h/c \in \{0.75, 1.0, 1.5\}$ (Ozdemir et al., 2021). Results were compared to a 2D geometry showing that the higher the aspect ratio, the closer the performance of a 3D wing operating close to the free surface is to that of a 2D wing. Yet, no finite wings provided the hydrodynamic characteristics of a 2D geometry.

Therefore, a gap remains in the understanding of the effects of aspect ratio on the performance of submerged hydrofoils, especially at high Froude numbers ($Fr_c > 3.0$), typical of actual foiling conditions. Hence, the present paper investigates the influence of wing aspect ratio and immersion depth on hydrofoils operating at low, moderate, and high velocities. In particular, it discusses the existence of a threshold value of aspect ratio from which a 3D wing would provide similar hydrodynamic characteristics to an infinite wing under the same operating conditions. The existence of such a threshold value would represent a step forward in reducing computational time when analyzing submerged 3D lifting surfaces.

For this purpose, the method is first described and the numerical framework is drawn in Section 2. Then, in Section 3, hydrofoil performance computed using a boundary element method (BEM) with the linearized Neumann-Kelvin condition for the free surface is analyzed with respect to flow velocity, submergence, and aspect ratio. It concludes on the possibility of predicting the performance of finite-span, shallowly-submerged hydrofoils by means of 2D simulations.

## 2 NUMERICAL METHOD

### 2.1 Strategy

Assuming that the performance of a 2D hydrofoil is equivalent to that of a hydrofoil of infinite aspect ratio, the hydrodynamic characteristics of a finite wing of aspect ratio $\Lambda$ can be equal to those of a 2D wing only if there exists a threshold value of aspect ratio $\Lambda_c$ above which hydrofoil performance is less than a given accuracy of a wing of infinite span. As such, this study investigates the existence of such a critical value of aspect ratio $\Lambda_c$ for different flow velocities and hydrofoil submergence. For this purpose, hydrofoil wings of aspect ratios between $4$ and $20$ were studied in different operating conditions using a 3D BEM code. In particular, three chord-based Froude numbers $Fr_c = 0.5$, $Fr_c = 1.1$, and $Fr_c = 6.3$ were analyzed, with

$$Fr_c = \frac{U_0}{\sqrt{gc}}, \tag{1}$$

where $U_0$ is the undisturbed flow velocity in the $x$-direction, $g$ is the gravitational acceleration, and $c$ is the hydrofoil root chord length.

The first Froude number is subcritical. $Fr_c = 1.1$ corresponds to a moderate flow velocity and $Fr_c = 6.3$ is seen as a high Froude number. Concerning immersion depth, a wide range of submergence depth-to-chord ratios $h/c$ between $0.1$ and $30$ were swept. The angle of attack $\alpha$ remained constant and was set to $+2°$. Table 1 summarizes the operating conditions investigated in this paper.

**Table 1. Operating conditions.**

| $Fr_c$ [-] | $U_0$ [m/s] | $\alpha$ [°] | $h/c$ [-] |
|---|---|---|---|
| 0.5 | 0.6 | 2 | 0.1–30 |
| 1.1 | 1.2 | 2 | 0.1–30 |
| 6.3 | 7.0 | 2 | 0.1–30 |

## 2.2 Problem Formulation

A descriptive scheme of the flow around a shallowly-submerged hydrofoil is presented in Figure 1. The immersion depth was defined at the mid-chord of the center-line, the same as the center of rotation of the angle of attack. The submergence depth-to-chord ratio is defined between this point and the free surface at rest $z = 0$.

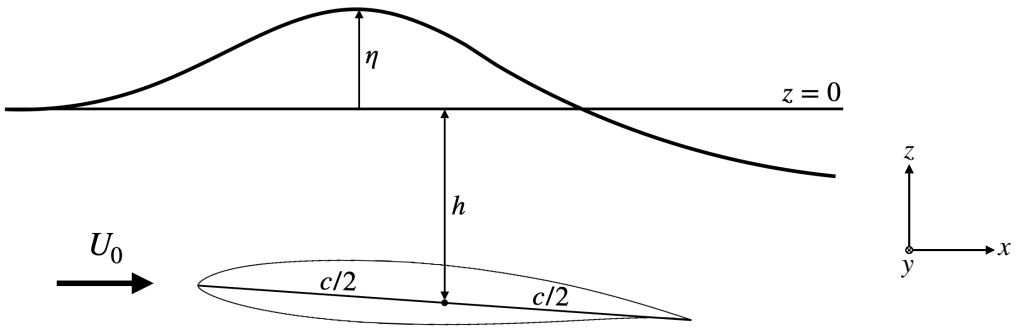


**Figure 1. Schematic description of the problem.**

## 2.3 Numerical Model

The fluid problem was addressed using *PUFFIn*[1], a 3D potential flow solver based on a BEM approach. The solver *PUFFIn* is detailed in Perali et al. (2023) and the theoretical framework used in the present work only for steady simulations is recalled here.

The fluid flow is considered incompressible and irrotational, and viscous effects are neglected. The velocity field $\boldsymbol{u}$ is the superposition of the undisturbed velocity $\boldsymbol{U_0}$ with the gradient of the perturbation potential $\phi$. It satisfies Laplace's equation

[1] https://www.ensta-bretagne.fr/en/optifoil

$$\boldsymbol{\nabla}^2 \phi = 0. \tag{2}$$

Applying the second Green identity to this equation yields the following boundary integral equation (Katz and Plotkin, 2001):

$$\phi = -\frac{1}{4\pi} \int_S \left[ \sigma \frac{1}{r} - \mu \, \boldsymbol{n} \cdot \boldsymbol{\nabla} \left( \frac{1}{r} \right) \right] dS, \tag{3}$$

where $\sigma$ are the sources and $\mu$ are the doublets such that

$$\sigma = -\frac{\partial \phi}{\partial n}, \quad \mu = -\phi. \tag{4}$$

$S$ is the domain boundary, which typically consists of the body surface $S_B$, the wake surface $S_W$, and the free-surface boundary $S_{FS}$. $\boldsymbol{n}$ is the outward pointing vector normal to $S$. Under the assumption that the wake should not support hydrodynamic loads, the source distribution on $S_W$ is null. Consequently, Equation 3 can be rewritten:

$$\phi = -\frac{1}{4\pi} \int_{S_B + S_{FS}} \left[ \sigma \frac{1}{r} - \mu \, \boldsymbol{n} \cdot \boldsymbol{\nabla} \left( \frac{1}{r} \right) \right] dS + \frac{1}{4\pi} \int_{S_W} \left[ \mu \, \boldsymbol{n} \cdot \boldsymbol{\nabla} \left( \frac{1}{r} \right) \right] dS, \tag{5}$$

with the sources $\sigma$ given by the non-penetration condition on the hydrofoil

$$\sigma = -\boldsymbol{U_0} \cdot \boldsymbol{n}. \tag{6}$$

Furthermore, *PUFFIn* models the free surface either by a linearized Neumann-Kelvin, a symmetry condition, or an antisymmetry condition resulting from the asymptotic behaviors of the Froude number $Fr_c \longrightarrow 0$ and $Fr_c \longrightarrow \infty$, respectively (Newman, 2018). In the scope of this paper, simulations were run using the Neumann-Kelvin formulation linearized at $z = 0$

$$\left( \boldsymbol{U_0} \cdot \boldsymbol{\nabla} \right)^2 \phi + g \frac{\partial \phi}{\partial z} = 0. \tag{7}$$

To solve the problem numerically, the boundaries are discretized using quadrilateral elements. The distribution of sources and doublets is assumed constant on each element. Writing Equation 5 at the geometrical center of each element yields a general matrix form (Filippas and Belibassakis, 2014)

$$\boldsymbol{A}(\eta) \begin{bmatrix} \boldsymbol{\mu_B} \\ \\ \boldsymbol{\sigma_{FS}} \end{bmatrix} = \boldsymbol{B}(\eta) \begin{bmatrix} \boldsymbol{\sigma_B} \\ \\ \boldsymbol{\mu_{FS}} \end{bmatrix} + \boldsymbol{W}(\eta) \, \boldsymbol{\mu_W}, \tag{8}$$

where $\eta$ is the free-surface elevation such that

$$\eta = -\frac{1}{g}\, \boldsymbol{U_0} \cdot \boldsymbol{\nabla}\phi. \tag{9}$$

$\boldsymbol{\sigma_B}$ and $\boldsymbol{\mu_B}$ denote the sources' strength and doublets' strength on the body, respectively. Likewise, $\boldsymbol{\sigma_{FS}}$ and $\boldsymbol{\mu_{FS}}$ denote the sources' strength and doublets' strength on the free surface, respectively. $\boldsymbol{\mu_W}$ corresponds to doublets' strength on the wake panels. $\boldsymbol{\sigma_B}$ is provided by Equation 6 while the other strength vectors are unknown. $\boldsymbol{A}(\eta)$, $\boldsymbol{B}(\eta)$, and $\boldsymbol{W}(\eta)$ can be computed for constant-strength singularity panels. Considering the linearized free-surface condition 7, the problem is solved by inverting $\boldsymbol{A}(\eta)$ once at the beginning of the computation, using a lower-upper decomposition.

A Lagrangian approach is used to construct the wake surface during the computation. The process is iterative in time. That is, the position of a wake panel at the current time step is obtained from the value of the velocity at the previous time step. Since the flow is considered inviscid, the potential on a wake panel convected by the flow remains constant. Hence, $\boldsymbol{\mu_W}$ only depends on the strength of the doublets on the panels located downstream of the trailing edge. The latter is computed by imposing an equality of pressure between the suction side and the pressure side (i.e., a Kutta condition) at the trailing edge of the hydrofoil.

Pressure distribution on the body is yielded by the Bernoulli relation. From there, the hydrodynamic forces and moments acting on the hydrofoil are computed by integrating the pressure over the surface $S_B$. Simulations end when a residual criterion on the last $N$ iterations is met. The criterion is defined such that the maximum deviation on forces is $0.005$ N for the last $N = 20$ iterations.

The size of the free surface domain is dependent on the foil chord length. Upstream of the foil was left a distance of 5 chords while downstream of the foil was 200 chord lengths. Port and starboard, the distance to foil tips was 20 times the chord such that the hydrofoil was centered in the transverse direction of the flow.

Simulations were run in steady conditions. As observed by Prasad et al. (2015), wave-breaking can occur at low submergence, thus causing unsteadiness responsible for fluctuation in lift and drag. Since viscous effects are neglected in *PUFFIn*, such a phenomenon is not captured by the solver. Additionally, unsteadiness in the wake of the hydrofoil may occur in the close vicinity of the free surface, especially at subcritical Froude numbers. Despite not accounting for such phenomena, the results provide an overview of the evolution of lift and drag in close proximity to the free surface.

### 2.4 Geometry

The lifting surfaces under study were chosen rectangular to avoid accumulating effects induced by more complex geometries and rather focus on the influence of the sole aspect ratio. Their cross-section profile is an H105 profile (Speer, 2001), which is very close to most sections used in foil design. The zero-lift angle of the H105 profile is $\alpha_0 = -2.35°$. In the framework of this research, appendages were generated using *LEModeler*[2], an open-source code for modeling parametric hydrofoil geometries developed for the purpose of this study, using the *Rhinoceros*® CAD engine.

[2] https://github.com/hu4o-nicolas/LEModeler

### 2.5 Mesh Definition and Convergence

Geometries have been meshed with structured grids refined at the leading and trailing edges. To capture 3D effects, the spanwise panel distribution was refined to leave smaller square cells at foil tips, especially close to the leading edge. The reference mesh was set up on the hydrofoil of $\Lambda = 4$ at ($h/c = 20$, $Fr_c = 6.3$) and further adapted to the lifting surfaces of a higher aspect ratio while leaving the chord fixed and equal to $c = 0.125$ m. That is, the number of panels spanwise was changed proportionally to the span while keeping the same mesh topology than $\Lambda = 4$. The results of the mesh convergence on lift coefficient are shown in Figure 2. Subsequently, a mesh of 1280 panels ($16$ panels spanwise and $40$ along the chord on each side) was selected as the reference to balance cost and accuracy. A 3D view of the reference geometry is visible in Figure 3.

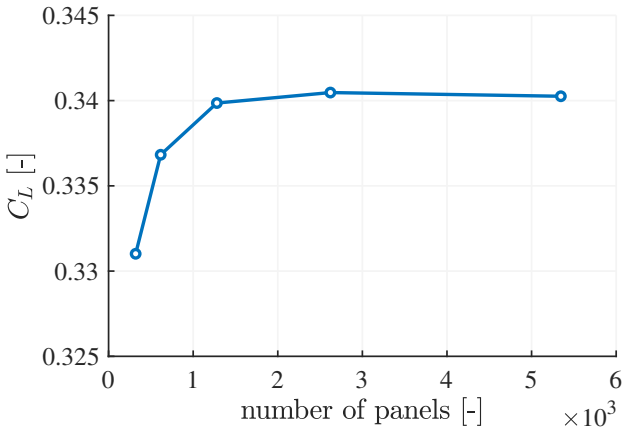


**Figure 2. Mesh convergence on $C_L$ ($\Lambda = 4$, $Fr_c = 6.3$, and $h/c = 20$).**

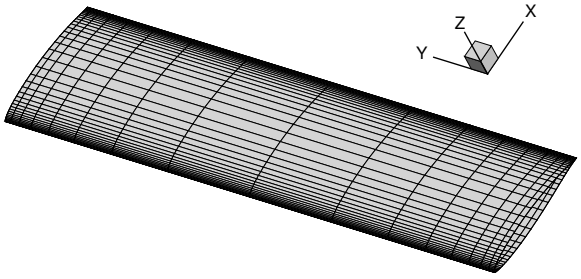


**Figure 3. Reference mesh ($\Lambda = 4$).**

## 3 RESULTS

### 3.1 Influence of the Free Surface

For the three chord-based Froude numbers at stake (i.e., $Fr_c = 0.5$, $Fr_c = 1.1$, and $Fr_c = 6.3$), BEM simulations were run on finite wings $\Lambda \in \{4, 6, 10, 20\}$ for different submersion depths between $h/c = 0.1$ and $h/c = 30$. The resulting lift and drag coefficients (total drag) are visible in Figure 4.

The lift coefficient appears to plummet when approaching too close to the free surface, no matter the flow velocity. As discussed above, the values of lift and drag in close proximity to the free surface (typically $h/c < 0.5$ here) must be taken with caution since unsteadiness may occur. Yet, the significant lift reduction is in agreement with the literature, which justifies the use of steady BEM for

providing an overview of hydrofoil performance near the free surface.

The evolution in lift coefficient between subcritical and supercritical Froude numbers is well captured by the simulations. The case at $Fr_c = 0.5$ exhibits a bump close to $h/c = 1.0$, which is consistent with the literature on subcritical Froude numbers. The bump provides a lift increase up to $15.8\%$ for ($Fr_c = 0.5$, $\Lambda = 20$), which shows the potential benefit of operating in the vicinity of the free surface for maximizing hydrofoil lift. For $Fr_c = 1.1$, a portion of the peak remains from $h/c = 3.0$ for the larger wings. For $Fr_c = 6.3$, it is made clear that the peak disappeared completely. Such an evolution reveals a change in the curve trend of the lift coefficient versus submergence between subcritical and supercritical Froude numbers. The proximity to the free surface induces a systematic reduction of the lift coefficient at supercritical Froude numbers, which is consistent with other studies when inertial forces dominate.

When reducing the submergence, at $Fr_c = 0.5$, the drag first decreases until $h/c = 2.0$ before sharply rising up. At high Froude numbers, the drag first increases until $h/c = 1.5$ and then decreases. These variations are more pronounced for the highest aspect ratio. The occurrence of the peak and the decrease in drag coefficient is delayed to greater submergence by increasing the flow velocity. Furthermore, the amplitude of the peak is lowered with increasing speed, due to the reduction in wave drag with speed. The maximum amplitude is obtained at ($h/c = 0.1$, $Fr_c = 0.5$, $\Lambda = 20$), where the drag coefficient rises up to $C_D = 0.06$.

The convergence of each force curve with submergence reveals that the threshold $h/c$ at which infinite depth behavior is reached depends on the Froude number. Here, the effects of the free surface vanish for $h/c$ higher than around $10$ at a low Froude number and for $h/c$ higher than around $25$ at the highest Froude number. The existence of such a threshold value of submergence is largely observed in the literature, as discussed above. Past that critical value, a change in aspect ratio acts as an offset on the lift and drag coefficients.

### 3.2 Influence of Wing Aspect Ratio

Figure 5 shows the evolution of the force coefficients normalized by their value ($C_{L_0}$ and $C_{D_0}$) obtained for $\Lambda = 20$ and $h/c = 30$, where there is no more influence of the free surface. Each figure in 5 corresponds to a given value of submergence. $h/c = 1.0$ refers to the immersion at which a lift bump is observed in Figure 4. $h/c = 3.0$ was selected as an intermediate case, where the effects of the free surface remain significant yet reduced. Finally, $h/c = 5.0$ shows the evolution of lift and drag when only a small proportion of the effects of free surface persists. At $h/c = 30$, the free surface and Froude number effects are null. Consequently, the curves of $C_L/C_{L_0}$ and $C_D/C_{D_0}$ with respect to $\Lambda$ at $Fr_c = 0.5$, $Fr_c = 1.1$, and $Fr_c = 6.3$ superimpose. For each submergence, the case at $h/c = 30$ is thus drawn and serves as a reference for comparison.

The positive slope of each lift curve reveals that the lift coefficient increases with the aspect ratio for all simulations. On the other hand, a negative curve slope illustrates that the drag coefficient decreases with an increase in aspect ratio. By comparing the force coefficients at different $h/c$, it appears clear that the higher the submergence, the closer the lift coefficient to the reference curves.

The evolution of the lift and drag coefficients at $h/c = 1.0$ illustrates that the effects of flow velocity are substantial in the vicinity of the free surface. The lift curve for $Fr_c = 0.5$ is strictly higher than that provided by any other flow regime. It is positioned strictly above the reference curve, which means that (1) the free-surface proximity is beneficial to the lift coefficient, and (2) the bump in the lift observed in Figure 4 for $h/c = 1.0$ provides the highest lift coefficient over any other operating condition. This behavior is in agreement with the evolution of the lift coefficient with the Froude num-

ber at $h/c = 1.0$ observed in the literature. That further illustrates the potential benefit of operating near the free surface at low speed. For higher velocities, at $h/c = 1.0$, the lift coefficient increases with speed. However, since their value is below the case at $h/c = 30$, the free-surface proximity appears detrimental to hydrofoil lift at high Froude numbers. At $h/c = 1.0$, the drag coefficient is part of the sharp drag peak observed in Figure 4. At that water depth, the evolution of the drag coefficient for $Fr_c = 1.1$ is singular. As opposed to the latter, the drag curves for $Fr_c = 0.5$ and $Fr_c = 6.3$ show a detrimental impact of free-surface proximity on hydrofoil drag. For any other operating condition simulated, the drag coefficient decreases as the aspect ratio increases, as observed in Figure 4.

For $h/c = 3.0$ and $h/c = 5.0$, the lift curves at $Fr_c = 0.5$ and $Fr_c = 1.1$ superimpose for all the aspect ratios. Similar behavior is observed for drag at $h/c = 5.0$ only. That is, the Froude number has no influence from low to moderated speeds once the effects of free surface diminish. At $Fr_c = 6.3$, however, the effects of the Froude number remain. Therefore, the effects of free surface persist longer at high velocity. Yet, they appear mitigated by reducing $\Lambda$. This behavior illustrates the increase with the aspect ratio of the threshold value of submergence from which the effects of free surface become negligible. As opposed to the case $Fr_c = 6.3$, the cases $Fr_c = 0.5$ and $Fr_c = 1.1$ show a slight benefit of operating near the free surface at higher submergence when free-surface effects remain. It is worth noting the change from detrimental to beneficial of the lift coefficient for $Fr_c = 1.1$. Overall, the free surface acts as a mere reduction in hydrofoil performance at high speed, while it may be beneficial at low and moderate Froude numbers.

### 3.3 Lift and Drag Convergence with Aspect Ratio

Slope variation for all curves in Figure 5 illustrates that the lift and drag coefficients asymptote by increasing the aspect ratio, no matter the operating conditions. Most importantly, the proximity with the free surface demonstrates the capability of accelerating the convergence of the lift and drag coefficients with respect to the aspect ratio systematically at a high Froude number. As a result, the critical value of aspect ratio $\Lambda_c$ may be drastically lowered by free-surface proximity with respect to that at an infinite water depth. For example, the increase in lift coefficient between $\Lambda = 10$ and $\Lambda = 20$ at ($Fr_c = 6.3$, $h/c = 3.0$) is $8.97\%$. At an infinite water depth, the increase would be $11.6\%$. A similar trend leading to similar conclusions is observed for drag. This suggests the feasibility of assessing the hydrodynamic coefficients of a wing of finite span under specific operating conditions close to the free surface by means of 2D simulations. In particular, the variation of lift and drag at $Fr_c = 6.3$ suggests the existence of a relation for determining $\Lambda_c$ as a function of the Froude number, the submergence depth-to-chord ratio, and the aspect ratio for high-speed operating conditions.

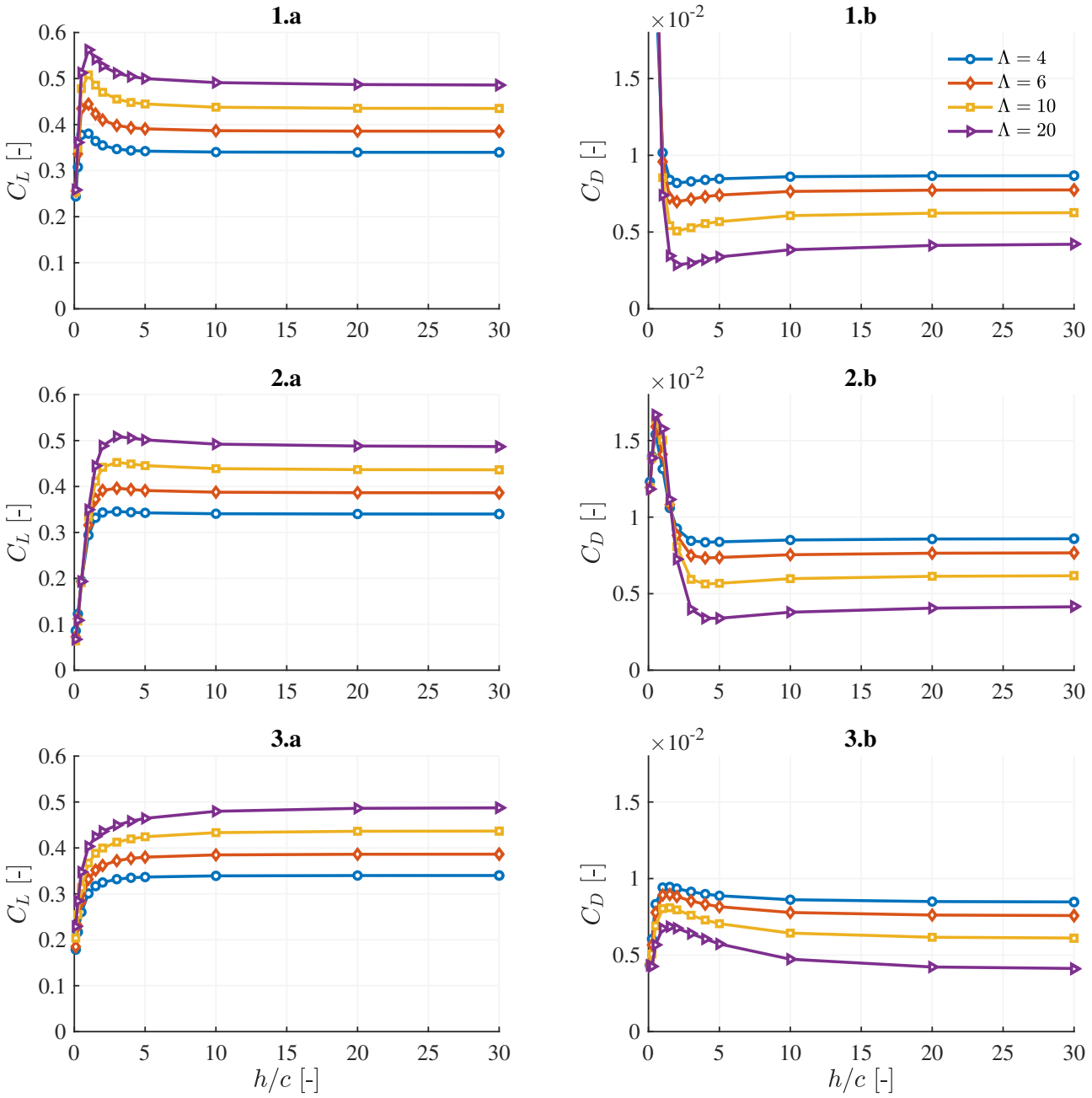


**Figure 4. (a) Lift and (b) drag coefficient with respect to submergence depth-to-chord ratios for wings of different aspect ratios at (1) $Fr_c = 0.5$, (2) $Fr_c = 1.1$, and (3) $Fr_c = 6.3$.**

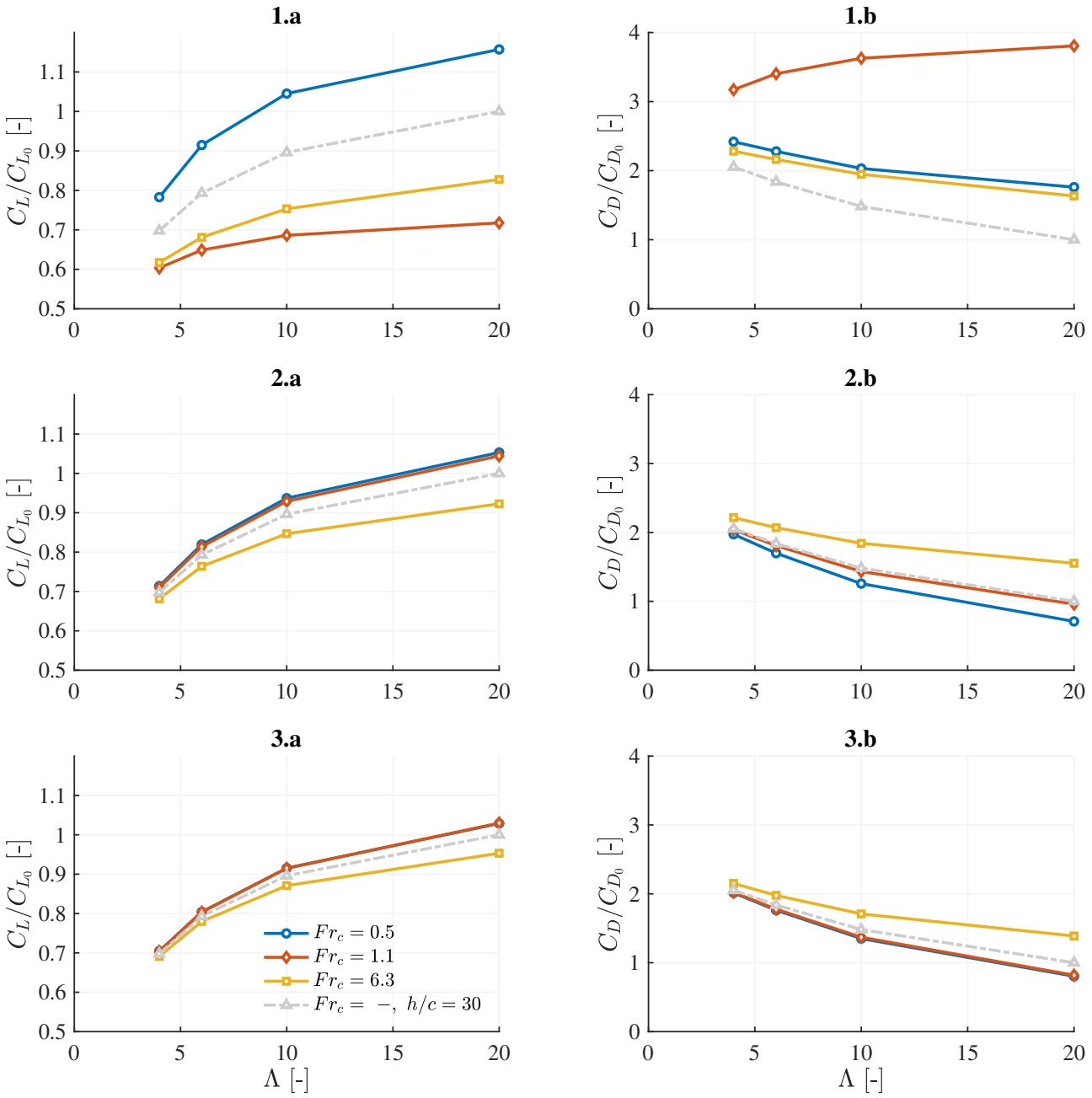


**Figure 5. Normalized (a) lift and (b) drag coefficient with respect to wing aspect ratio for different chord-based Froude numbers at (1) $h/c = 1.0$, (2) $h/c = 3.0$, and (3) $h/c = 5.0$.**

## 4 CONCLUSIONS

In an effort to save computational costs, the present paper addresses the feasibility of using 2D models to retrieve the hydrodynamic characteristics of finite hydrofoils operating beneath the free surface. To do so, simulations on fully-submerged rectangular wings of variable aspect ratios under different flow velocities and immersion depths are performed using a 3D boundary element method with a linearized Neumann-Kelvin condition for the free surface. The difference between subcritical and supercritical Froude numbers is well captured by the flow solver, which demonstrates the applicability of steady panel methods to the problem of fully-submerged hydrofoils of variable aspect ratios operating near the free surface.

Several conclusions may be drawn from the present work:

- The influence of the free surface increases with the aspect ratio.
- The effects of the Froude number at low submergence are substantial and diminish with immersion, up to the point that they disappear when the effects of free surface vanish.
- The immersion value above which the effects of free surface vanish is delayed with flow velocity and aspect ratio.
- At $Fr_c = 6.3$, the proximity with the free surface accelerates the convergence of the lift and drag coefficients with respect to the aspect ratio.

Complementary analyses of local quantities (e.g. pressure coefficients, free-surface elevation, effective angles of attack) are required to explain the variations of the lift and drag coefficients discussed in this paper. Additionally, further investigations should determine the range of operating conditions under which similar behavior to that at $Fr_c = 6.3$ is observed and state a formal equation for determining $\Lambda_c$ as a function of $h/c$ and $Fr_c$.

All in all, this work lays the first stones for further understanding the influence of geometric parameters on the performance of closely-submerged hydrofoils in view of performing multi-fidelity optimizations, for example.

## REFERENCES


Ali, A. and M. Karim (2010). “Numerical Study of Free Surface Effect on the Flow Around Shallowly Submerged Hydrofoil”. In: *Proceedings of MARTEC 2010 The International Conference on Marine Technology*. Vol. 11, p. 12.

Bai, K. J. (1978). “A Localized Finite-Element Method for Two-Dimensional Steady Potential Flows with a Free Surface”. In: *Journal of Ship Research* 22.04, pp. 216–230. ISSN: 0022-4502. DOI: 10.5957/jsr.1978.22.4.216.

Bal, S. (2007). “High-Speed Submerged and Surface Piercing Cavitating Hydrofoils, Including Tandem Case”. In: *Ocean Engineering* 34.14, pp. 1935–1946. ISSN: 0029-8018. DOI: 10.1016/j.oceaneng.2007.03.007.

Bal, S., S. A. Kinnas, and H. Lee (2001). “Numerical Analysis of 2-D and 3-D Cavitating Hydrofoils Under a Free Surface”. In: *Journal of Ship Research* 45, pp. 34–49. DOI: 10.5957/jsr.2001.45.1.34.

Binns, J. R., P. A. Brandner, and J. Plouhinec (2008). “The Effect of Heel Angle and Free-Surface Proximity on the Performance and Strut Wake of a Moth Sailing Dinghy Rudder T-foil”. In: The 3rd High Performance Yacht Design Conference. Auckland, NZ.

Carabineanu, A. (2014). “The Study of the Potential Flow Past a Submerged Hydrofoil by the Complex Boundary Element Method”. In: *Engineering Analysis with Boundary Elements* 39, pp. 23–35. ISSN: 0955-7997. DOI: 10.1016/j.enganabound.2013.10.017.

Chen, Z. (2012). “A Vortex Based Panel Method for Potential Flow Simulation around a Hydrofoil”. In: *Journal of Fluids and Structures* 28, pp. 378–391. ISSN: 0889-9746. DOI: 10.1016/j.jfluidstructs.2011.10.003.

Daskovsky, M. (2000). “The Hydrofoil in Surface Proximity, Theory and Experiment”. In: *Ocean Engineering* 27.10, pp. 1129–1159. ISSN: 00298018. DOI: 10.1016/S0029-8018(99)00032-3.

Duncan, J. H. (1983). “The Breaking and Non-Breaking Wave Resistance of a Two-Dimensional Hydrofoil”. In: *Journal of Fluid Mechanics* 126, pp. 507–520. ISSN: 1469-7645, 0022-1120. DOI: 10.1017/S0022112083000294.

Faltinsen, O. M. (2005). *Hydrodynamics of High-Speed Marine Vehicles*. Cambridge University Press. ISBN: 978-0-521-84568-7.

Farell, C. (1973). “On the Wave Resistance of a Submerged Spheroid”. In: *Journal of Ship Research* 17.01, pp. 1–11. ISSN: 0022-4502. DOI: 10.5957/jsr.1973.17.1.1.

Filippas, E. S. and K. A. Belibassakis (2014). “Hydrodynamic Analysis of Flapping-Foil Thrusters Operating beneath the Free Surface and in Waves”. In: *Engineering Analysis with Boundary Elements* 41, pp. 47–59. ISSN: 0955-7997. DOI: 10.1016/j.enganabound.2014.01.008.

Giesing, J. P. and A. M. O. Smith (1967). “Potential Flow about Two-Dimensional Hydrofoils”. In: *Journal of Fluid Mechanics* 28.1, pp. 113–129. ISSN: 0022-1120. DOI: 10.1017/S0022112067001934.

Havelock, T. H. (1929). “The Vertical Force on a Cylinder Submerged in a Uniform Stream”. In: *Proceedings of the Royal Society of London. Series A, Containing Papers of a Mathematical and Physical Character*. Vol. 122, pp. 387–393. DOI: 10.1098/rspa.1929.0028.

Hoque, A., M. Karim, and Aevelina Rahman (2017). “Simulation of Water Wave Generated by Shallowly Submerged Asymmetric Hydrofoil”. In: *Procedia Engineering*. 10th International Conference on Marine Technology, MARTEC 2016 194, pp. 38–43. ISSN: 1877-7058. DOI: 10.1016/j.proeng.2017.08.114.

Hough, G. R. and J. P. Moran (1969). “Froude Number Effects on Two-Dimensional Hydrofoils”. In: *Journal of Ship Research* 13.01, pp. 53–60. ISSN: 0022-4502. DOI: 10.5957/jsr.1969.13.1.53.

Jego, C. (2022). “CFD Investigation of the Impact of the Free Surface Proximity on the Performances of a T-shaped Olympic Class Kitefoil Hydrofoil”. MA thesis. University of Southampton.

Karim, M., B. Prasad, and N. Rahman (2014). “Numerical Simulation of Free Surface Water Wave for the Flow around NACA 0015 Hydrofoil Using the Volume of Fluid (VOF) Method”. In: *Ocean Engineering* 78, pp. 89–94. ISSN: 0029-8018. DOI: 10.1016/j.oceaneng.2013.12.013.

Katz, J. and A. Plotkin (2001). *Low-speed aerodynamics*. Vol. 13. Cambridge university press.

Kennell, C. and A. Plotkin (1984). “A Second-Order Theory for the Potential Flow About Thin Hydrofoils”. In: *Journal of Ship Research* 28.01, pp. 55–64. ISSN: 0022-4502. DOI: 10.5957/jsr.1984.28.1.55.

Kwag, S. and K. Mori (1991). “Numerical Simulation of Free-Surface Flows around 3-D Submerged Hydrofoil by N-S Solver”. In: *Journal of the Society of Naval Architects of Japan* 1991.170, pp. 93–102. DOI: 10.2534/jjasnaoe1968.1991.170_93.

Michel, W. H., S. F. Hoerner, and L. W. Ward (1954). *Hydrofoil Handbook Volume II - Hydrodynamic Characteristics of Components*. Technical report. New York 6, NY: Gibbs & Cox, Inc.

Newman, J. N. (2018). *Marine Hydrodynamics*. The MIT Press. ISBN: 9780262534826.

Ni, Z., M. Dhanak, and T. Su (2021). “Performance of a Hydrofoil Operating Close to a Free Surface over a Range of Angles of Attack”. In: *International Journal of Naval Architecture and Ocean Engineering* 13, pp. 1–11. ISSN: 20926782. DOI: 10.1016/j.ijnaoe.2020.11.002.

Ozdemir, Y. H., T. Cosgun, and B. Barlas (2021). “Wave Field Generated by Finite-Span Hydrofoils Operating beneath a Free Surface”. In: *Brodogradnja: Teorija i praksa brodogradnje i pomorske tehnike* 72.1, pp. 145–167. ISSN: 0007215X, 18455859. DOI: 10.21278/brod72108.

Parkin, B. R., B. Perry, and T. Y. Wu (1955). *Pressure Distribution on a Hydrofoil Running near the Water Surface*. 47-2. American Institute of Physics.

Patterson, N. and J. Binns (2022). “Development of a Six Degree of Freedom Velocity Prediction Program for the Foiling America’s Cup Vessels”. In: *Journal of Sailing Technology* 7.01, pp. 120–151. ISSN: 2475-370X. DOI: 10.5957/jst/2022.7.6.151.

Perali, P. et al. (2023). “Comparison of Viscous and Potential Flow Predictions for the Performances of a Hydrofoil near the Free Surface”. In: *Ocean Engineering* (IN REVIEW).

Pernod, L. et al. (2023). “Free-Surface Effects on Two-Dimensional Hydrofoils by RANS-VOF Simulations”. In: *Journal of Sailing Technology* 8.01, pp. 24–38. ISSN: 2475-370X. DOI: 10.5957/jst/2023.8.2.24.

Plotkin, A. (1975). “The Thin-Hydrofoil Thickness Problem Including Leading-Edge Corrections”. In: *Journal of Ship Research* 19.02, pp. 122–129. ISSN: 0022-4502. DOI: 10.5957/jsr.1975.19.2.122.

Prasad, B., T. Hino, and K. Suzuki (2015). “Numerical Simulation of Free Surface Flows around Shallowly Submerged Hydrofoil by OpenFOAM”. In: *Ocean Engineering* 102, pp. 87–94. ISSN: 00298018. DOI: 10.1016/j.oceaneng.2015.04.049.

Speer, T. E. (2001). “The BASILICUS Project - Return of the Cruising Hydrofoil Sailboat”. In: *Chesapeake Sailing Yacht Symposium*. SNAME 15th Chesapeake Sailing Yacht Symposium. Annapolis, Maryland, USA, pp. 1–22. DOI: 10.5957/CSYS-2001-013.

Thiart, G. D. (2001). “Generalized Vortex Lattice Method for Prediction of Hydrofoil Characteristics”. In: *R&D Journal* 17.2.

Uddin, I. and M. Karim (2017). “Application of Volume of Fluid (VOF) Method for Prediction of Wave Generated by Flow around Cambered Hydrofoil”. In: *Procedia Engineering*. 10th International Conference on Marine Technology, MARTEC 2016 194, pp. 82–89. ISSN: 1877-7058. DOI: 10.1016/j.proeng.2017.08.120.

Wadlin, K. L., C. L. Shuford Jr., and John R. McGehee (1952). *A Theoretical and Experimental Investigation of the Lift and Drag Characteristics of Hydrofoils at Subcritical and Supercritical Speeds*. Technical report 1232. Langley Field, Va.: National Advisory Committee for Aeronautics.

Xie, N. and D. Vassalos (2007). “Performance Analysis of 3D Hydrofoil under Free Surface”. In: *Ocean Engineering* 34.8, pp. 1257–1264. ISSN: 0029-8018. DOI: 10.1016/j.oceaneng.2006.05.008.

Yasko, M. (1998). “Boundary Element Method for a Hydrofoil near the Free Surface”. In: *Engineering Analysis with Boundary Elements* 21.2, pp. 191–194. ISSN: 0955-7997. DOI: 10.1016/S0955-7997(98)00010-1.

Yeung, R. W. and Y. C. Bouger (1979). “A Hybrid Integral-Equation Method for Steady Two-Dimensional Ship Waves”. In: *International Journal for Numerical Methods in Engineering* 14.3, pp. 317–336. ISSN: 1097-0207. DOI: 10.1002/nme.1620140303.

Zhu, Q., Y. Liu, and K. P. Y. Dick (2006). “Dynamics of a Three-Dimensional Oscillating Foil Near the Free Surface”. In: *AIAA Journal* 44.12, pp. 2997–3009. ISSN: 0001-1452, 1533-385X. DOI: 10.2514/1.21617.